Structure of the helium isotopes ^{4}He$-^8$He

Jürgen Wurzer[*] and Hartmut M. Hofmann

Institut für Theoretische Physik III, Staudtstraße 7, Universität Erlangen-Nürnberg, D-91058 Erlangen, Germany

Ground state wave functions of the halo nuclei ^{6}He and ^{8}He have been determined by a genetic algorithm in the framework of the refined resonating group model. The genetic algorithm allows one to apply the underlying variational principle to very complex wave functions and to extract their most important structures in order to give a physical interpretation. The spectrum of the particle unstable isotopes $^{A+1}$He$_{N+1}$ has been determined from the phase shifts of neutron scattering on the particle stable nuclei ^{A}He$_N$. Stepwise going on, using the same NN potential in the refined resonating group method bound state and scattering calculation, yielded a consistent description of the nuclei ^{4,5,6,7,8}He. [S0556-2813(97)04601-3]

I. INTRODUCTION

Since it had been realized that the nucleus ^{6}He has a halo character like, e.g., ^{11}Li a lot of theoretical investigations have been performed on it, e.g., [1–9]. This is on the one hand due to the obviously simple structure, a strongly bound α core interacting with two weakly bound neutrons [10] and on the other hand due to the importance of the nn pairing for the binding of the ^{6}He nucleus. This means that ^{6}He seems to be a perfect candidate for a three particle calculation, especially because the effective αn interaction is much better known than the very ambiguous ^{9}Li n interaction which is needed for calculations on ^{11}Li. And indeed most investigations on this nucleus are using a macroscopic three particle model [1,3,4,6,7].

These calculations are able to reproduce most ground state properties of ^{6}He very well, but it turned out that they all lack binding energy by about 0.5 MeV. This might be due to the missing triton-triton structure which can cure this underbinding in microscopic multichannel cluster model calculations [8]. Recently, the Greens Function Monte Carlo approach was used to study $A=6$ nuclei [9].

Only a little attention was paid to ^{8}He (e.g., [11]) which can no more be regarded as a ^{6}He-n-n three body system due to the weak binding of ^{6}He. A proper description of ^{8}He seems only possible in the framework of a microscopic cluster model.

In this work we present a first attempt to describe the particle stable nuclei ^{4,6,8}He and the particle unstable systems ^{5,7}He on the same footing. An effective NN potential fitted to the most important NN phase shifts and not adjusted to the different systems was used in a microscopic cluster model, the refined resonating group method (RRGM) [13].

The realization of the very time consuming underlying variational calculation for nonlinear parameters, especially for ^{8}He, was only possible by using a newly developed numerical method based on a genetic algorithm [14].

The paper is organized in the following way: in Sec. II we give a brief survey of the RRGM and a few remarks on the

NN potential used. In Secs. III to VII we describe details of the calculations and their results for the systems ^{4}He to ^{8}He. Finally, Sec. VIII contains a discussion and an outlook.

II. THE METHOD

In the following we present a brief summary of the formal basics of the refined resonating group method. Details are given in [13,15]. The Schrödinger equation for the bound states is solved by Ritz variational principle with the ansatz

$$\Psi = \mathcal{A}\phi^j, \tag{1}$$

$$\phi^j = \left[\sum_{l,s,k} c_{l,s,k}\varphi_k^l \Xi^s\right]^j, \tag{2}$$

which consists of spin-isospin functions Ξ^s and orbital functions φ_k^l. The spin s and the orbital angular momentum l are coupled to j. The sum k may run over different fragmentations, different sets of orbital angular momenta, and different sets of width parameters (see below). $\mathcal{A}$ denotes the total antisymmetrization operator. The orbital part consists of a product of cluster internal functions $\varphi_{k,a,\text{int}}$ and cluster relative functions $\varphi_{k,b,\text{rel}}^l$

$$\varphi_k^l = \left(\prod_{a=1}^{n_c} \varphi_{k,a,\text{int}}\right)\left(\prod_{b=1}^{n_c-1} \varphi_{k,b,\text{rel}}^l\right), \tag{3}$$

$$\varphi_{k,a,\text{int}} = \exp\left(-\frac{\beta_{k,a}}{n_a}\sum_{i<j}^{n_a}(\mathbf{r_i}-\mathbf{r_j})^2\right), \tag{4}$$

$$\varphi_{k,b,\text{rel}}^l = \exp(-\gamma_{k,b}s_k^2)\mathcal{Y}_l(\mathbf{s}_k), \tag{5}$$

where n_c is the number of clusters, n_a is the number of nucleons in cluster a, $\mathbf{r_i}-\mathbf{r_j}$ are relative coordinates within a cluster; $\mathbf{s}_k$ denotes the cluster relative coordinates in Jacobian form and $\mathcal{Y}_l(\mathbf{x}) = x^l Y_{lm}(\hat{\mathbf{x}})$ is a solid spherical harmonic. Clusters containing only one nucleon are described by

---

*Electronic address: jwurzer@theorie3.physik.uni-erlangen.de

TABLE I. Coefficients of the added singlet odd central potential.

$A_c^{1-,1}$	$=$	100.0 MeV	$B_c^{1-,1}$	$=$	4.8092 fm^{-2}
$A_c^{1-,2}$	$=$	115.0 MeV	$B_c^{1-,2}$	$=$	0.6409 fm^{-2}
$A_c^{1-,3}$	$=$	-20.0 MeV	$B_c^{1-,3}$	$=$	0.4430 fm^{-2}
$A_c^{1-,4}$	$=$	1.1 MeV	$B_c^{1-,4}$	$=$	0.0500 fm^{-2}

$\varphi_{k,a,\text{int}} = 1$. The variational parameters are the coefficients $c_{l,s,k}$ and the width parameters $\beta_{k,a}$ and $\gamma_{k,b}$.

For the scattering problem the Kohn-Hulthén variational procedure [15] is used with the ansatz

$$\Psi_n = \mathcal{A}\left\{ \sum_m \phi_{m,1}^{j_1}\phi_{m,2}^{j_2} \frac{Y_{L_{\text{rel},m}}}{R_{\text{rel}}}\left[\delta_{nm}F_m(R_{\text{rel}}) + a_{nm}\widetilde{G}_m(R_{\text{rel}}) \right. \right.$$
$$\left. \left. + \sum_l b_{lmn}\chi_{lm}(R_{\text{rel}}) \right] \right\}, \tag{6}$$

where F_m and $\widetilde{G}_m$ are the regular and regularized irregular Coulomb functions and χ_{lm} are square integrable functions of Gaussian type. R_{rel} is the modulus of the relative vector between the two scattered fragments. The variational parameters a_{nm} and b_{lmn} are determined by requiring that

$$\delta(\langle\Psi_n|H-E|\Psi_n\rangle - \tfrac{1}{2}a_{nn}) = 0. \tag{7}$$

The $\phi_{m,i}^{j_i}$ describing the two fragments and assuming to be fixed during the scattering process are bound states of the form (2) and determined before performing the actual scattering calculation.

The Hamiltonian contains a kinetic energy term and an extended version of the nucleon-nucleon interaction of Stöwe and Zahn [16], which has been successfully applied in the description of some Li and Be isotopes [16–18] and various reactions, e.g., ^{2}H(d,γ)^{4}He [19]. This potential was designed by fitting the most important NN phase shifts and consists of a Coulomb, central, spin-orbit, and tensor component. However, it does not contain an odd contribution in the central component. Such a term was negligible for the nuclei, which had been studied before with the original version of the potential, but it turned out that for neutron halo nuclei, due to the many pairs of nucleons in relative odd states, an odd contribution in the central part, which is mainly repulsive, is no longer negligible [20] in order to prevent an overbinding. Therefore, we added a singlet-odd term to the original version. This term was determined by fitting the $^1P_1$ NN phase shift from SAID [22]. Its radial dependence is given by a sum of Gaussian functions:

$$V_c^{1-}(r) = \sum_{i=1}^4 A_c^{1-,i}\exp(-B_c^{1-,i}r^2). \tag{8}$$

The coefficents $A_c^{1-,i}$ and $B_c^{1-,i}$ are given in Table I. The extended version of the potential was successfully used in the description of the ^{10}Li system [23].

In the discussion of our results for the scattering calculations, we use the usual parametrization of the calculated S matrix

$$S_{kl}(E) = \eta_{kl}(E)e^{2i\delta_{kl}(E)}, \tag{9}$$

in terms of phase shifts $\delta_{kl}(E)$ and channel coupling strength $\eta_{kl}(E)$. In addition to the diagonal phase shifts $\delta_{ll}(E)$, we use the eigenphases $\widetilde{\delta}_l(E)$ defined by

$$\widetilde{S}_{kl}(E) = \sum_{ij} U_{ki}S_{ij}(E)U_{jl}^* = \delta_{kl}e^{2i\widetilde{\delta}_l(E)} \tag{10}$$

to study resonances.

To extract the resonant part of the eigenphases, we calculated also a (hard sphere) background phase shift

$$\tan\delta_l^{\text{bg}} = \frac{F_l(kR)}{G_l(kR)}, \tag{11}$$

and subtracted it from the eigenphases. The value of the hard sphere radius R is discussed in Sec. VI.

For the particle stable systems we have calculated the r.m.s. matter $\langle\Psi|\hat{r}^2|\Psi\rangle^{1/2}$ and charge radii and the matter

$$\rho(\mathbf{r}) = \langle\Psi|\hat{\rho}(\mathbf{r})|\Psi\rangle, \tag{12}$$

$$\hat{\rho}(\mathbf{r}) = \sum_{j=1}^N \delta(\mathbf{r}_j - \mathbf{r}), \tag{13}$$

and charge density distributions.

III. THE NUCLEUS ^{4}He

The ^{4}He wave function in our model consists of a simple Gaussian function in order to simplify the calculations for the heavier isotopes, where we want to use it as an α core. The width parameter $\beta = 0.2793$ fm^{-2} determined by variation corresponds to a point nucleon matter radius of 1.42 fm which, if folded by a nucleon matter distribution of $\langle r^2\rangle^{1/2} = 0.8$ fm, agrees very well with the experimental value of 1.67 ± 0.01 fm [24], but the binding energy is only -21.18 MeV instead of the experimentally determined -28.296 MeV [25]. This remarkable lack of binding is not a real problem because we are interested only in threshold and excitation energies relative to bound state energies, and for the effect on the structure of the nuclei it is only important that the binding of the α cluster is large compared to the interaction between other clusters and the α cluster.

The width of the α cluster in the particle stable helium isotopes is not constrained to the width of the ^{4}He, but determined by variation in order to take into account the effects of the presence of the other nucleons.

A further justification for the use of such a simple wave function consisting just of one Gaussian are the differential cross sections for elastic proton ^{4}He scattering (Fig. 1), calculated by a Glauber model [26] on the basis of the ^{4}He
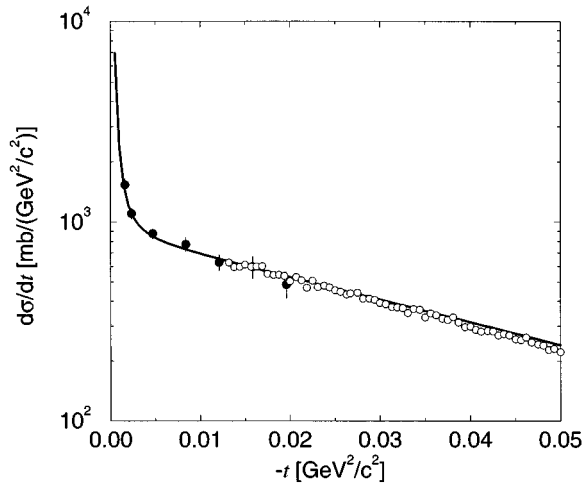
FIG. 1. Differential cross sections for elastic proton ^{4}He scattering versus squared four momentum transfer $-t$, calculated by a Glauber model [26] on the base of the ^{4}He RRGM density distribution (line) compared with the data [27,28] (dots) and [29] (circles).

RRGM density distribution, which agree very well with the experimentally measured cross sections [27–29]. For that purpose the RRGM point nucleon density distribution was folded by a nucleon matter distribution of $\langle r^2 \rangle^{1/2} = 0.8$ fm.

IV. THE ^{5}He SYSTEM

^{5}He is particle unstable with respect to neutron emission with 0.89 MeV [30]. A broad excited $J^\pi = 1/2^-$ state is situated 4 ± 1 MeV above the $3/2^-$ ground state. The second excited state lies at 16.75 MeV just above the second threshold (^{3}H$+d$). Obviously, the natural ground state structure is α-n in a relative P wave. Therefore, we have performed a scattering calculation for elastic neutron scattering off the ^{4}He nucleus with $L_{rel} = 1$ as a first test on the suitability of our NN interaction on the helium isotopes. In Fig. 2 the resulting phase shifts are shown in comparison with the experimental ones [31]. The agreement with data is reasonable
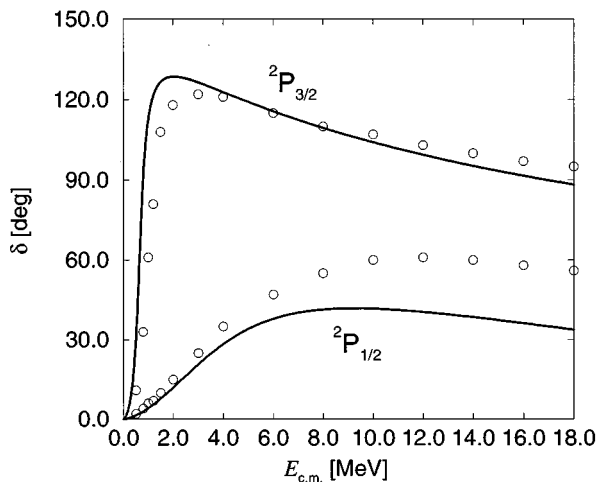

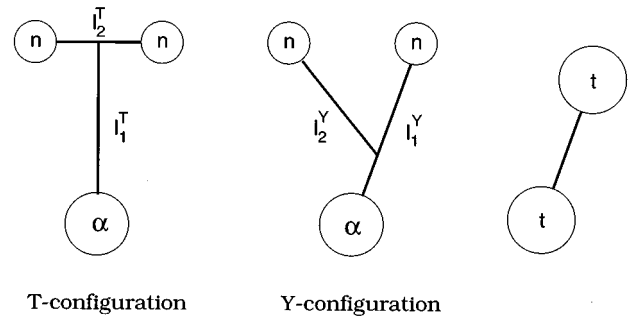FIG. 2. Calculated ^{4}He$+n$ scattering phase shifts (full lines) in comparison with data (circles) [31].

FIG. 3. Representations of the two different sets of Jacobi coordinates for the α-n-n clustering and the triton-triton clustering.

as expected from other calculations with similar simple wave functions [32], but would be much better if one would, additionally, take into account the triton-deuteron channel. Neglecting higher partial waves and the inelastic reaction into the triton-deuteron channel does not allow the reproduction of the higher excited states. The too strong splitting between the $3/2^-$ and $1/2^-$ phase shifts in Fig. 2 indicates that for the employed model space, the spin-orbit potential is too strong.

V. THE HALO NUCLEUS ^{6}He

The nucleus ^{6}He is bound with 0.975 MeV with respect to three particle break up into ^{4}He$+2n$ [30]. The fact that each two of these three components are unbound shows the importance of the pairing of the dineutron system for the binding of ^{6}He. The quantum numbers of the ground state are $J^\pi = 0^+$. The first excited state at 1.80 MeV is 2^+. The ^{3}H$+^3$H threshold is situated 12.307 MeV above the ground state.

Nowadays ^{6}He is called a halo nucleus [10,33], but the halo character of its structure has only been identified after one recognized its similarity to ^{11}Li, one of the first nuclei for which these exotic structures had been realized [34]. In analogy with ^{11}Li the ground state configuration of ^{6}He is assumed to be a three particle system consisting of an almost inert α core and a two neutron halo. Tanihata et al. [10], e.g., supported this statement by showing that the relation

$$\sigma_{-2n}(^6\text{He}) = \sigma_I(^6\text{He}) - \sigma_I(^4\text{He}) \qquad (14)$$

for the two neutron removal cross section σ_{-2n} and the interaction cross section σ_I of the helium isotopes on a carbon target at $800A$ MeV is satisfied within the experimental error bars. This relation was deduced by Ogawa et al. [35] by applying a Glauber model to a loosely bound system. Therefore, most theoretical investigations on ^{6}He are based on a macroscopic three particle model. Ground state properties like r.m.s. radii and matter densities are well described by these models, but they all miss about 0.5 MeV in binding energy. This indicates that ^{4}He$+2n$ is the most important configuration, but there is at least one other important structure.

There are two different sets of Jacobi coordinates in a macroscopic three particle model or a microscopic three cluster model. They are displayed in Fig. 3 and according to their appearance are called Y and T configuration [7] in the

TABLE II. Binding energy E_B, matter $\langle r_m^2 \rangle^{1/2}$, and charge $\langle r_{ch}^2 \rangle^{1/2}$ r.m.s. point nucleon radii and excitation energy E^* to the 2^+ state for the ^{6}He wave functions compared with data. N is the number of nonlinear variational parameters. $Y_{l_1 l_2}$ denotes the Y configuration with relative angular momenta l_1 and l_2, analogous is the meaning of $T_{l_1 l_2}$, tt abbreviates the triton-triton clustering.

	Configuration	N	E_B (MeV)	$\langle r_m^2 \rangle^{1/2}$ (fm)	$\langle r_{ch}^2 \rangle^{1/2}$ (fm)	E^* (MeV)
$wf1$	Y_{11}	9	unbound	-	-	-
$wf2$	$Y_{11}+Y_{00}$	9	0.17	2.48	1.78	0.91
$wf3$	$Y_{11}+Y_{00}$	18	0.37	2.51	1.79	1.40
$wf4$	$Y_{11}+Y_{00}+$tt	23	1.02	2.38	1.80	1.98
$wf5$	$Y_{11}+Y_{00}+$tt	13	0.74	2.35	1.77	2.06
$wf6$	$Y_{11}+Y_{00}+$tt	13	0.85	2.38	1.80	2.02
$wf7$	$Y_{11}+Y_{00}+$tt$+T_{00}+T_{11}$	23	1.12	2.36	1.79	2.16
exp.			0.975 [30]	2.33±0.04 [10]	1.72±0.04 [10]	1.80 [30]

following. In principle the variational spaces spanned by the Y and T configurations are equivalent, provided an infinite number of relative angular momenta l_1 and l_2 and width parameters are allowed, but if one restricts the relative angular momenta, e.g., to S and P waves, and the number of width parameters, like we did, they will in general span different variational spaces which overlap only partially. For $l_{1,2}=0,1$ the variational space for the T configuration is smaller because of the Pauli principle which forbids odd values for l_2^T if $S=0$ and even values for $S=1$. This yields two basis functions, i.e., possible angular momentum couplings per set of width parameters instead of three as for the Y configuration.

Therefore, we started our investigations on ^{6}He with an α-n-n three cluster Y configuration with P waves only on the relative coordinates, according to Table II called $wf1$, and following the notation of [11] specified by $Y_{l_1 l_2}= Y_{11}$. Using up to four Gaussians on each relative coordinate, did not yield any binding. Adding S waves ($wf2$) leads to a binding of 0.11 MeV for four Gaussians per relative coordinate. Doubling the number of nonlinear variational parameters by using two separate sets of width parameters (β_k,γ_k) for S and P waves ($wf3$) increases the binding to 0.37 MeV. The α width in the parameter set for the P waves turned out to be 0.3148 fm^{-2}, which means a small decrease of the α cluster radius compared to the ^{4}He nucleus, but for the S wave set, the α width decreased to 0.1415 fm^{-2}, a value which means that the α cluster is about as large as the whole nucleus, indicating that the clustering α-n-n is not a proper description or at least not the only one for the six nucleons in relative S waves. An alternative clustering would be a triton-triton configuration with $l=0$ (cf. Fig. 3). The addition of such a configuration with four Gaussians on the relative coordinate ($wf4$) increases the binding to a realistic value of 1.02 MeV. Obviously, the triton-triton configuration is very important for the binding. The triton cluster width in $wf4$ is determined to 0.2647 fm^{-2} leading to a smaller radius as for the free triton nucleus which has a width parameter of 0.2077 fm^{-2}. The widths of the α clusters are 0.1571 fm^{-2} and 0.3157 fm^{-2} for the S- and P-wave sets. In order to use the ^{6}He wave function as a core in ^{8}He or as a bound state fragment in the ^{7}He scattering calculation, we tried to simplify it by reducing the number of Gaussians per relative coordinate. Only two Gaussians per coordinate ($wf5$) re-

duces the binding energy to 0.74 MeV.

But the still very small value of the α width in the S wave set of $wf4$ and $wf5$ calls for a better description of the triton-triton structure. Using, therefore, two Gaussians for the triton clusters, as it is usually done for the description of the triton [36,37], but only one for their relative coordinate ($wf6$), i.e., without changing the size of the variational space, improves the binding of $wf5$ by more than 100 keV, and increases the width of the α in the S wave set in $wf6$ to 0.2262 fm^{-2}. Omitting the S wave set in $wf6$ reduces the binding by about only 200 keV, so that we can conclude that the α-n-n clustering with $l_{1,2}=1$ and the triton-triton clustering are the most important structures for the ^{6}He nucleus.

The T configuration with P waves only is unbound like the Y one was. T, triton-triton, and Y configurations with relative S and P waves and two Gaussians on each relative coordinate (except for the triton-triton), i.e., $wf6$ with additional corresponding T configuration, yields a binding energy of 1.12 MeV ($wf7$), but this increase in the binding compared to $wf6$ is not an indication of the importance of the T configuration, it rather reflects the increase of the dimension of the variational space for the nonlinear parameters from 13 to 23. Therefore, one better should compare the binding of $wf7$ with the one of $wf4$ which has a variational space of the same dimension (cf. Table II). An important reason for the 100 keV stronger binding of $wf7$ compared to $wf4$ might be the description of the triton by two Gaussians in $wf7$. So we conclude that the T configuration can be omitted if enough width parameters per coordinate are used in the other configurations.

Table III shows the remaining binding energy for $wf7$ if one omits each one of the configurations in order to deter-

TABLE III. Remaining binding energy for $wf7$ omitting each one of the configurations.

Omitted component	E_B (MeV)
none	1.12
Y_{00}	0.95
Y_{11}	unbound
tt	0.35
T_{00}	0.93
T_{11}	0.97
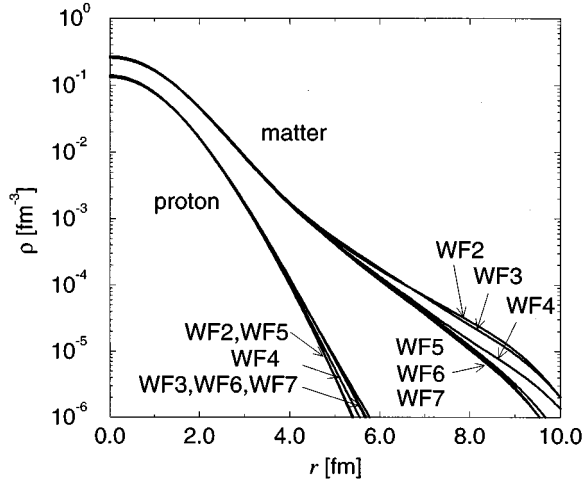
FIG. 4. Calculated matter and charge density distributions for the ^{6}He wave functions.

FIG. 5. Differential cross sections for elastic proton ^{6}He scattering versus squared four momentum transfer $-t$, calculated by a Glauber model [26] on the base of the ^{6}He RRGM density distribution for $wf6$ (line) compared with data (dots) [27,28].

mine the importance of each configuration. Without Y_{11} the binding is lost. Omitting the triton-triton clustering decreases the binding considerably. The other configurations contribute hardly at all. These results are in agreement with Csótó [8] who also identified the Y_{11} and triton-triton configurations as the most important ones in a microscopic description. In the calculations of Varga et al. [11], who consider a variational space containing only T_{00}, Y_{00}, and Y_{11} configurations, the Y_{11} is also the most important one, followed by T_{00} and then Y_{00}. Without taking into account a triton-triton clustering, they got a binding energy of 1.016 MeV by adjusting the exchange parameter u of their simple NN potential, which contains only a central nuclear force.

Comparing the values for the radii in Table II reveals that the matter and charge radii for the wave functions $wf4$ to $wf7$, the ones with realistic values for the binding energy, are almost identical and in good agreement with data, but also for the just weakly bound functions $wf2$ and $wf3$, the radii are close to the experimental upper bound.

The excitation energy E^* to the 2^+ state was determined by calculating the lowest eigenvalue of the Hamiltonian for wave functions with the same width parameters as for the ground state, but with angular momentum couplings necessary for $J^\pi=2^+$. This procedure was necessary because even this first excited state is unbound and, therefore, no variation of the width parameters is possible. Performing a scattering calculation like for ^{5}He in order to determine the phase shifts would, because of the three particle break up of the lowest ^{6}He threshold, in principle requires the handling of a scattering wave function with three fragment asymptotics which is not yet possible in the RRGM. Again the excitation energies for the functions $wf4$ to $wf7$ are almost identical and in reasonable agreement with the experimental value.

Also, the density distributions shown in Fig. 4 do not vary for the functions $wf4$ to $wf7$ up to 8 fm. As one would expect, the function $wf4$ with the largest number of Gaussians per relative coordinate from this set of four functions drops a bit slower than the others because of the better asymptotic description which is enabled by this larger freedom in the variational space. For $wf2$ and $wf3$ the much weaker binding yields a slower decrease in the density distribution.
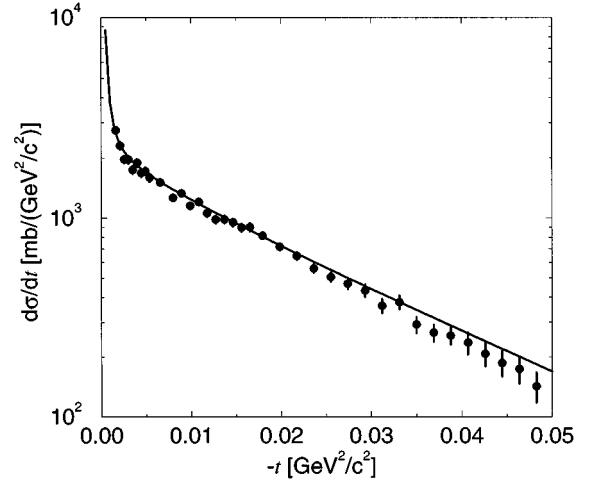
Using these densities, folded by the nucleon size of 0.8 fm, the differential cross sections for elastic proton scattering off ^{6}He have been calculated via a Glauber model [26]. They are in good agreement with data. Figure 5 shows, e.g., the calculated cross sections for $wf6$ compared with the experimental results of [27,28]. Using two width parameters instead of one for the α-cluster yields even better agreement, especially in the range of large momentum transfer $-t$ [28]. For the ^{8}He wave functions, two α width parameters cannot be employed because of the huge amount of computing time necessary. Therefore, we restrict ourselves in this work on one α width parameter in order to give a consistent description of the helium isotopes from $A=4$ to $A=8$.

VI. THE ^{7}He SYSTEM

The nucleus ^{7}He is particle unstable with respect to neutron emission with 0.44 MeV [30,38]. The ground state quantum numbers are $J^\pi=3/2^-$ ($1p^{3/2}$). The corresponding $1p^{1/2}$ doublet partner or other excited states are not observed until now [38]. To calculate the spectrum of this system, we considered elastic neutron scattering off the ^{6}He ground state and transitions into the first excited state up to a center-of-mass energy of 20 MeV. The energy spectrum is deduced from a phase shift analysis. The other possible channels, ^{4}He$+3n$, ^{5}He$+2n$, and ^{3}He$+^3$H$+n$ with thresholds 0.535, 1.43, and 11.867 MeV above the ^{7}He ground state are three or four particle break up reactions. In order to simplify the calculation, we used the ^{6}He ground state wave function $wf6$ and the corresponding wave function for the ^{6}He 2^+ excited state and restricted the relative angular momentum of the neutron to $L_{rel} \leq 2$. This leads to the following number n of coupled channels per J^π value:

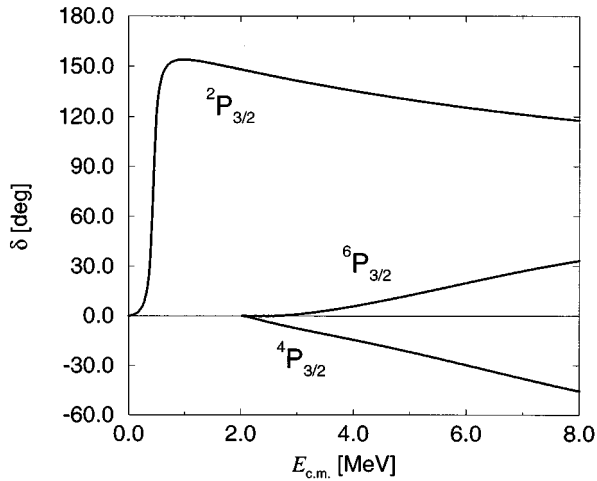| J^π	$\frac{1}{2}^-$	$\frac{3}{2}^-$	$\frac{5}{2}^-$	$\frac{1}{2}^+$	$\frac{3}{2}^+$	$\frac{5}{2}^+$
n	2	3	2	3	4	4

FIG. 6. The $\frac{3}{2}^-$ ^{6}He-n and ^{6}He*-n diagonal phase shifts.

In the following all resonance energies are given with respect to the ^{6}He+n threshold. The $3/2^-$ phase shifts in Fig. 6 show a narrow ($\Gamma = 0.12$ MeV) resonance at $E_{\rm res} = 0.45$ MeV in the elastic $^2P_{3/2}$ channel in excellent agreement with data [30] ($E_{\rm res} = 0.44$ MeV, $\Gamma_{\rm c.m.} = 160 \pm 30$ keV). A very broad $1/2^-$ resonance never reaching 90° due to a repulsive background phase appears in the $^2P_{1/2}$ channel (Fig. 7). To extract the resonant part of the phase shift, and so the resonance position, is a delicate task in this case. In order to get an estimate of the position of the hidden resonance, the background phase shift has to be approximately known. The only reproducible way known to us is to use hard sphere phase shifts, Eq. (11), for a given channel radius R, a procedure adopted from the recent compilation of ^{4}He in [25]. Unfortunately, the value of the hard sphere radius is essential, but it is not known. But for values of 5 to 7 fm for the hard sphere channel radius, a region in accordance with R-matrix analysis of similar light nuclei [25], the resulting resonance energies are situated between 2.75 and 4.25 MeV
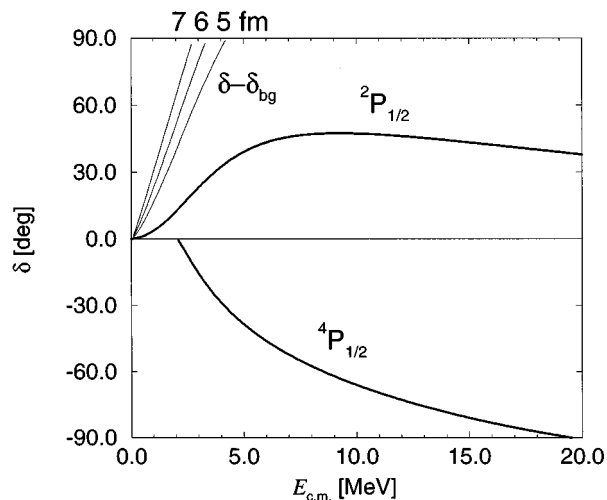
TABLE IV. Comparison of the resonance energies of excited states of ^{7}He determined in the present work for different hard sphere radii R with a shell model calculation. In order to facilitate the comparison of the calculations, the energies in the table are given with respect to the calculated ground state energy of ^{7}He contrary to the text. The shell model ground state is as in the present work $3/2^-$.

J^π	Present work			Shell model [39]	
	R (fm)			model space	
	5.0	6.0	7.0	$(0+1)\hbar\omega$	$(0+2)\hbar\omega$
$\frac{1}{2}^-$	3.8	2.9	2.3	3.43	4.27
$\frac{1}{2}^+$	-	-	-	-	4.55
$\frac{5}{2}^-$	5.5	4.7	4.1	5.03	5.38
$\frac{3}{2}^-$	-	-	-	7.47	

(cf. Fig. 7), an interval small compared to the corresponding resonance widths

$$\Gamma = 2 \left(\frac{\partial \delta(E)}{\partial E} \right)^{-1} \Bigg|_{E=E_{\rm res}} \qquad (15)$$

between 3.6 and 5.4 MeV. Note that the resonance energies in Table IV are relative to the calculated $3/2^-$ ground state energy, in contrast to the values given above which are relative to the ^{6}He+n threshold.

A neutron in a P wave cannot be coupled to $J^\pi = 5/2^-$ with the ^{6}He ground state, but one can consider elastic P-wave neutron scattering off the first excited ^{6}He state. The corresponding phase shifts are shown in Fig. 8, where a broad resonance appears between 4.6 and 6.0 MeV in the $^4P_{5/2}$ channel with a width between 3.5 and 5.9 MeV which is again large compared to the uncertainty resulting from the unknown hard sphere radius.

The broad widths of the $1/2^-$ and $5/2^-$ resonances could explain why they had not been observed experimentally until now.

FIG. 7. The $\frac{1}{2}^-$ ^{6}He-n and ^{6}He*-n diagonal phase shifts and the corresponding resonant part of the eigenphase of the elastic channel for a hard sphere radius of 5, 6, and 7 fm.
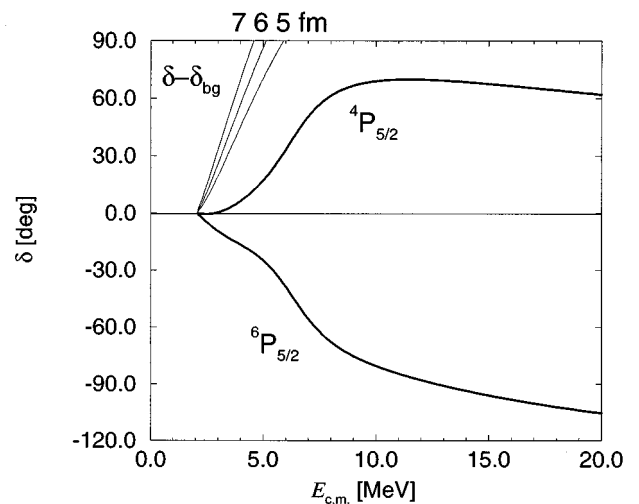
FIG. 8. The $\frac{5}{2}^-$ ^{6}He-n and ^{6}He*-n diagonal phase shifts and the corresponding resonant part of the eigenphase of the $^4P_{5/2}$ channel for a hard sphere radius of 5, 6, and 7 fm.
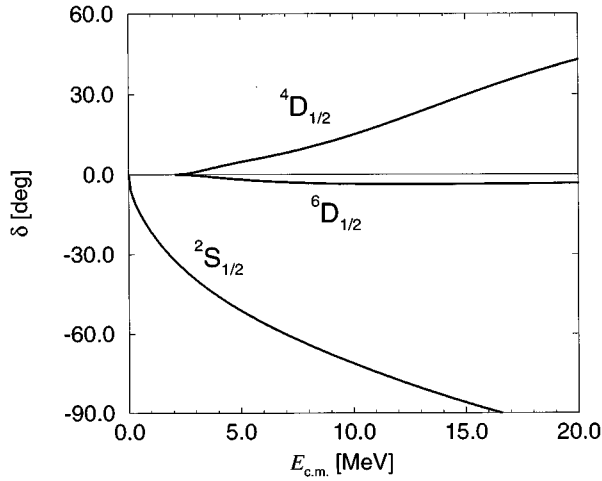
FIG. 9. The $\frac{1}{2}^+$ diagonal phase shifts for ^{6}He-n scattering.

FIG. 10. Representation of the four clusterings α-n-n-n-n, α-n-n-nn, α-nn-n-n, and α-nn-nn used in the ^{8}He functions.

The phase shifts for $L_{rel}=0$ and 2 are without any resonant structures. Therefore, we renounce to show them except for the ones for the quantum numbers $1/2^+$ in Fig. 9.

In Table IV we compare our results for the excited states with a shell model calculation [39]. Both in the $(0+1)\hbar\omega$ and the $(0+2)\hbar\omega$ model space agreement for the $1/2^-$ and $5/2^-$ states with the present work is obvious. The shell model ground state is $3/2^-$ as in our calculations, but in the shell model calculation, a further excited state appears: either a second $3/2^-$ in the $(0+1)\hbar\omega$ space or a positive parity state $(1/2^+)$ in the $(0+2)\hbar\omega$ space. In our phase shifts one can indeed recognize a very slow rising phase in the $^4D_{1/2}$ channel (cf. Fig. 9) and similarly a weakly attractive phase with the quantum numbers $3/2^-$ besides the ground state (cf. Fig. 6), but both cannot be called a resonance due to their weak energy dependence.

VII. THE HALO NUCLEUS ^{8}He

The nucleus ^{8}He is bound with 2.137 MeV against three particle breakup into ^{6}He$+2n$ [30]. The ν $1p^{3/2}$ shell is completely filled in ^{8}He which is the reason for its much stronger binding in comparison to ^{6}He. Other than the ground state, one excited state at 3.59 MeV with a width of $\Gamma=0.80$ MeV was recently identified as a 2^+ resonance [38].

Due to the weak binding of the nucleus ^{6}He, one cannot regard the ^{8}He as a mainly inert ^{6}He core surrounded by two further neutrons, rather one has to expect that the ^{6}He wave function is strongly modified, but the ^{4}He core should be

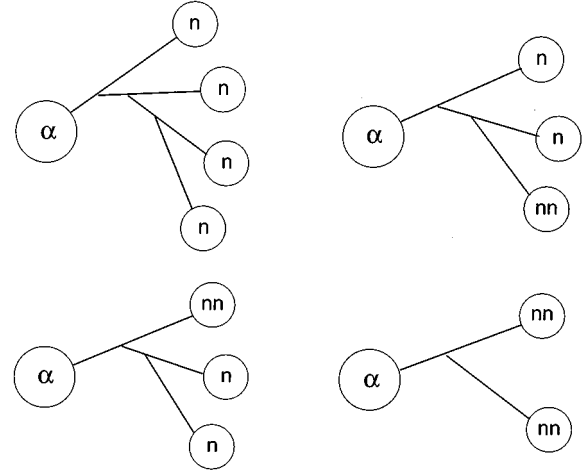still existing inside ^{8}He without large modifications. This assumption is in agreement with the fact that the relation corresponding to Eq. (14)

$$\sigma_{-2n}(^8\text{He}) = \sigma_I(^8\text{He}) - \sigma_I(^6\text{He}) \qquad (16)$$

does not hold for ^{8}He, but instead the equation

$$\sigma_{-2n}(^8\text{He}) + \sigma_{-4n}(^8\text{He}) = \sigma_I(^8\text{He}) - \sigma_I(^4\text{He}), \qquad (17)$$

which has also been derived by Ogawa et al. [35], holds very well [10].

Therefore, a ^{4}He$+4n$ structure for the description of the ^{8}He nucleus seems to be the proper choice. In order to simplify the calculation, but still retain enough freedom in the variation, we started with a function of the structure of ^{6}He-$wf3$, but only one Gaussian per relative coordinate instead of four and added two further neutrons on S or P waves, i.e., we used a superposition of the four structures α-n-n-n-n, α-n-n-nn, α-nn-n-n, and α-nn-nn (cf. Fig. 10). Here nn denotes dineutron clusters which are all in relative S waves. All single neutrons are in relative P waves. The possible angular momentum couplings are given in Table VI. We convinced ourselves that in the five cluster component, the part of the wave function with total spin $S=2$ almost does not contribute, hence, we omitted it as a further simplification of this still very complicated wave function, but even this simplified function ($WF1$) yields a binding of $E_{\text{Th}}=3.16$ MeV with respect to the ^{4}He$+4n$ threshold (cf. Table V), i.e., relative to the binding energy of the ^{4}He func-

TABLE V. Threshold energies E_{Th} and E'_{Th} (see text for details) to the ^{4}He$+4n$ breakup, matter $\langle r_m^2 \rangle^{1/2}$ and charge point nucleon $\langle r_{\text{ch}}^2 \rangle^{1/2}$ r.m.s. radii for the ^{8}He wave functions compared with data.

	E_{Th} (MeV)	E'_{Th} (MeV)	$\langle r_m^2 \rangle^{1/2}$ (fm)	$\langle r_{\text{ch}}^2 \rangle^{1/2}$ (fm)	$\langle r_m^2 \rangle^{1/2}/\langle r_{\text{ch}}^2 \rangle^{1/2}$
$WF1$	3.16	2.43	2.06	1.55	1.32
$WF2$	3.77	3.02	2.14	1.55	1.38
$WF3$	3.11	3.23	2.11	1.56	1.35
$WF4$	2.99	3.29	2.19	1.56	1.40
exp.	3.112 [30]		2.49±0.04 [10]	1.76±0.03 [10]	$1.41^{+0.05}_{-0.04}$

tion of Sec. III which consists of only one Gaussian. This is almost exactly the experimental value. The variational procedure yields α width parameters for WF1 of 0.3617 and 0.2937 fm^{-2} for the α-n-n-n-n and α-n-n-nn structures, which correspond to the P-wave set of the ^{6}He-$wf3$ core, and surprisingly large values for the α-nn-n-n and α-nn-nn structures, corresponding to the S-wave set of the ^{6}He-$wf3$ core, of 0.2508 and 0.2941 fm^{-2} in contrast to 0.1415 fm^{-2} in ^{6}He-$wf3$. In addition to E_{Th}, the binding energy relative to the energy of the one Gaussian ^{4}He function of Sec. III, we calculated the binding energy relative to a ^{4}He function consisting of four Gaussians with the α widths determined for ^{8}He-$WF1$, called E'_{Th} in Table V. Due to the stronger binding of the more complicated ^{4}He function $WF1$ is still lacking about 0.7 MeV of binding according to the value of E'_{Th}.

The radii of $WF1$ (cf. Table V) are much too small due to two reasons. The first one is the insufficient description of the asymptotic behavior of the wave function by only one Gaussian per relative coordinate. The second and much more serious problem is the effective NN potential employed which tends to lead to a too strong binding and too small radii for increasing mass number and number of clusters on relative P waves [20], but this is a common problem for all effective NN interactions known to us, usually avoided by adjusting some parameters of the potential. Since our interaction contains spin-orbit and tensor terms besides the central ones, it is not an easy task to adjust parameters of the potential for ^{8}He without destroying the agreement for the other isotopes completely. Our main goal is to find those configurations which determine the gross structure of ^{8}He. For ^{8}He the most interesting quantities are charge and matter radii in comparison to the ^{6}He quantities. Since these radii are strongly influenced by the separation energy, we present in the following results for model spaces which yield roughly the same binding energy, so that a comparison with data is possible. This choice of model spaces to avoid overbinding can be, however, only a preliminary solution as long as no better effective interaction is accessible. Since the construction of such a potential, which is just in work, is rather difficult, we have to postpone its application to a following publication.

We improved the asymptotic description of $WF1$ by adding a second Gaussian on the relative coordinate of the third and two further Gaussians on the relative coordinate of the fourth neutron in the five cluster structure ($WF2$), but because of the very complicated structure of this function — $WF2$ is the most complicated ^{8}He function considered, cf. Table VI — it was no more possible to determine the width parameters by variation even with the genetic algorithm method. Therefore, we retained the one width from $WF1$ unchanged and chose smaller values for the additional widths. We chose the additional parameters about a factor of 3 smaller, a factor found in the ^{6}He wave functions. Therefore, only the linear variation for the coefficients $c_{l,s,k}$ was carried out. This procedure yields a somewhat larger matter radius and 0.6 MeV increase in binding energy, cf. Table V.

In a next step we further simplified the structure of the wave function $WF1/WF2$ in order to be able to apply a variational procedure even with some additional width pa-

rameters. Therefore, we omitted the angular momentum couplings with negligible contributions to the binding energy. Omitting 20 out of the original 29 couplings (cf. Table VI) reduces the binding of $WF1$ by about 0.9 MeV, but then increasing the number of degrees of freedom for the ^{6}He core by adding one Gaussian on each coordinate of the core of the simplified function ($WF3$), we were able to perform a variation and got back the binding which was lost by reducing the number of couplings. In contrast to $WF1$ and $WF2$, where the α width parameters range from 0.2508 to 0.3617 fm^{-2}, in $WF3$ all α core parameters are about 10 percent larger than the one determined for the free ^{4}He (cf. Chapter III); therefore, the binding energy of a ^{4}He function with these four Gaussians is lower than the binding energy of the simple one Gaussian function by about 0.1 MeV. Therefore, here E_{Th} is 0.1 MeV smaller than E'_{Th}.

Repeating this process of omitting the unimportant structures on the one hand and increasing the degrees of freedom of the variation by increasing the number of the width parameters for the remaining structures on the other hand, we ended up with only four couplings, and only two clusterings (α-n-n-n-n and α-nn-n-n), but two Gaussians on each coordinate of the five cluster structure ($WF4$). In our model the most important ^{8}He components are three momentum couplings of the α-n-n-n-n five cluster structure (cf. Table VI) with each single neutron in a relative P wave, followed by the four cluster structure α-nn-n-n with an nn cluster in an S wave and the two neutrons in a P wave coupled to total orbital angular momentum $L=1$. This is in contradiction to the results of Varga et $al.$ [11,12], who also employed P waves, but only on the first and second coordinate of the structures α-n-n-n-n and α-n-n-nn. They found that these two structures yield the highest binding energies for all individual configurations, but omitting them from the total wave function hardly affected the binding energy [12]. They conclude a purely $l=0$ description containing the clusterings α-n-n-n-n, α-nn-n-n, and α-nn-nn with all neutrons and dineutron clusters in relative S waves is sufficient to describe the nucleus ^{8}He. It seems that this is due to their purely central potential which is adjusted to describe ^{6}He and ^{8}He in a model space which mainly contains relative angular momenta $l=0$.

The resulting radii of $WF4$ are still too small, but, moreover, our calculated radii for ^{8}He are even smaller than that for ^{6}He, cf. Tables II and V, which indicates a missing repulsion in our NN interaction.

This lack of repulsion is roughly a consequence of the soft core which is employed in all effective NN potentials in order to get a reasonable binding for light nuclei even with relative simple wave functions compared to the functions necessary for realistic interactions. This inevitably leads to an overbinding and to too small values for the radii of the nuclei at a certain number of nucleons due to the too high saturation point for the nuclear matter density of the effective potentials. The effect of the soft core increases with increasing number of nucleons, because of the increasing number of pair interactions, until finally the spatial volume occupied by a certain number of nucleons is smaller than the volume occupied by fewer nucleons like in this work for ^{8}He compared to ^{6}He. The same problem appears in the work of Varga et $al.$ [11,12].

TABLE VI. Couplings of angular momenta for the ^{8}He wave functions according to the coupling scheme $[[[l_1 l_2]^{l_{12}} l_3]^{l_{123}} l_4]^L$ and $[[[s_1 s_2]^{s_{12}} s_3]^{s_{123}} s_4]^S$ for the structure α-n-n-n-n and analogous for the other structures. Couplings marked with a + are used in the corresponding wave function. The numbers in parantheses are the numbers of nonlinear variational parameters. The number of basis functions, i.e., the number of coefficients $c_{l,s,k}$ is given in braces.

α-n-n-n-n	l_{12}	l_{123}	L	s_{12}	s_{123}	S	WF1 (5){24}	WF2 (5){144}	WF3 (7){20}	WF4 (9){28}
	0	1	0	1	1/2	0	+	+		
	1	1	0	1	1/2	0	+	+	+	+
	2	1	0	1	1/2	0	+	+		
	0	1	0	0	1/2	0	+	+	+	
	1	1	0	0	1/2	0	+	+		
	2	1	0	0	1/2	0	+	+	+	
	0	1	1	1	3/2	1	+	+		
	1	0	1	1	3/2	1	+	+	+	+
	1	1	1	1	3/2	1	+	+		
	1	2	1	1	3/2	1	+	+		
	2	1	1	1	3/2	1	+	+		
	2	2	1	1	3/2	1	+	+		
	0	1	1	1	1/2	1	+	+		
	1	0	1	1	1/2	1	+	+		
	1	1	1	1	1/2	1	+	+		
	1	2	1	1	1/2	1	+	+	+	+
	2	1	1	1	1/2	1	+	+		
	2	2	1	1	1/2	1	+	+		
	0	1	1	0	1/2	1	+	+		
	1	0	1	0	1/2	1	+	+		
	1	1	1	0	1/2	1	+	+		
	1	2	1	0	1/2	1	+	+		
	2	1	1	0	1/2	1	+	+		
	2	2	1	0	1/2	1	+	+		

α-n-n-nn	l_{12}	L	S	(5){2}	(5){2}	(7){4}
	0	0	0	+	+	
	1	1	1	+	+	+

α-nn-n-n	l_{12}	L	S	(5){2}	(5){2}	(7){8}	(5){1}
	1	0	0	+	+	+	
	1	1	1	+	+	+	+

α-nn-nn	L	S	(5){1}	(5){1}	(7){4}
	0	0	+	+	+

If one considers the ratio of the r.m.s. matter to r.m.s. charge radii in Table V, a good agreement with data is found for the wave function $WF4$, supporting the assumption that the remaining difference of the calculated values of the radii to the data is due to a lack of repulsion in the NN potentials and might not be curable by a further improvement in the description of the cluster relative motion.

Apart from this a further improvement of the wave function seems not possible at the moment because of the considerable amount of computing time required in performing the variational procedure. Only the application of a newly developed stochastic method of minimizing the ground state energy in variational calculations allowed us to perform the present work on ^{8}He at all. The only possible way until now to calculate a ^{8}He wave function in a microscopic model was to employ a very simple NN interaction. Varga *et al.* [11,12],

e.g., used a simple central nuclear force without spin-orbit or tensor component, also the Coulomb force was omitted. There are two important features of this genetic algorithm method which makes it superior to other search algorithms (like, e.g., the stochastic variational method discussed in [21]). Firstly, it is intrinsically parallel and can be used on parallel computers with any numbers of processors without any change, but contrary to other stochastic methods which are also working in a parallel way on a large number of processors, in the genetic algorithm the processors do not work independently from each other, rather they communicate after each function evaluation with each other. This leads to a kind of scaling behavior of the algorithm, i.e., increasing the number of processors by a factor x reduces the required real time for the variation also by a factor x. In usual stochastic methods, an increasing of the number of
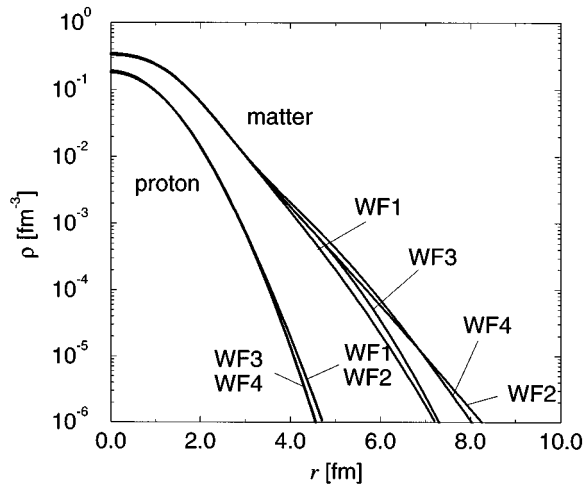
FIG. 11. Calculated matter and charge density distributions for the ^{8}He wave functions.

FIG. 12. Differential cross sections for elastic proton ^{8}He scattering versus squared four momentum transfer $-t$, calculated by a Glauber model [26] on the base of the ^{8}He RRGM density distribution for $WF4$ (line) compared with data (dots) [27,28].

processors only improves the statistics of the solutions but does not allow one to reduce the real time. Secondly, the variational space is not spanned by the variational parameters themselves, but by a bit representation of them, reducing strongly the possibility of getting trapped into a local minimum compared to other methods. For details see [14].

To get an idea of the effort necessary for the variational process, we give in Table VI in braces the number of basis functions, i.e., the dimension of the Hamiltonian matrices which have to be evaluated about a few 1000 times for each variation in order to determine reliably the nonlinear variational parameters the numbers of which are also given in parentheses. We emphasize that each element of these matrices has the structure $\langle \Psi_n | H | \Psi_m \rangle$ where Ψ_n is a complex eight particle wave function.

The first excited state of the ^{8}He nucleus is unbound and, therefore, a determination of its wave function by a variational procedure for the width parameters is again not possible. An attempt to describe this 2^+ state anologous to ^{6}He by the same Gaussian functions, but with different couplings failed completely for ^{8}He. The resulting excitation energies are about 10 MeV, far beyond the data, indicating that the ^{8}He 2^+ structure differs much more from the ^{8}He ground state than the ^{6}He 2^+ from the ^{6}He ground state. The variational space for the linear parameters $c_{l,s,k}$ which is determined by the simplified ground state ^{8}He wave functions is too small to describe the excited state properly. It might also be an indication for some deficiencies of the potential.

The calculated density distributions in Fig. 11 demonstrate that the larger the number of Gaussians describing the relative motion, the slower the decrease of the corresponding wave function at larger distances. Especially the much slower decrease for $WF2$ and $WF4$ compared to $WF1$ and $WF3$ emphasizes the importance of an adequate description for the relative motion of the last two neutrons.

In Fig. 12 the experimentally determined cross sections for elastic proton scattering at ^{8}He [27,28] are compared with the cross sections calculated on the basis of our density distribution for $WF4$, folded by the nucleon size, in a Glauber model [26]. The agreement is not so good as it was
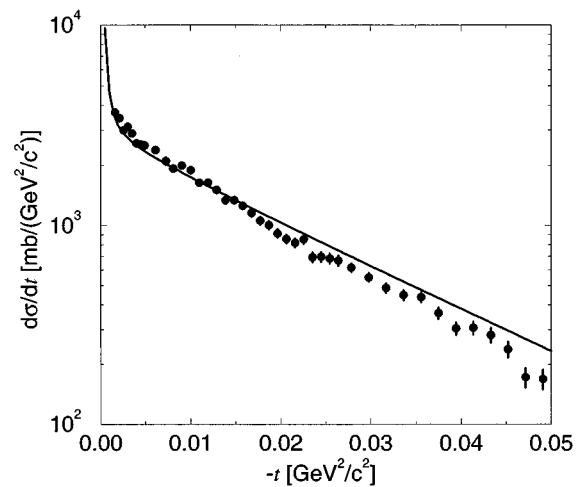
the case for ^{6}He. However, it is better than for $WF1$ and $WF3$, reflecting again the still not sufficient quality in the asymptotic description of the ^{8}He wave functions.

VIII. CONCLUSION

We have presented a first attempt to a unified microscopic description of the particle stable isotopes ^{4,6,8}He and the particle unstable systems ^{5,7}He using one effective parameter-free NN interaction not adapted to the different systems.

Using a newly developed genetic algorithm [14], it was possible to vary the nonlinear parameters of ^{8}He wave functions containing up to five clusters even for a complex NN interaction.

The ground state root mean square matter and charge radii, binding energy, and density distributions of the particle stable systems are in good agreement with data. For the ^{8}He nucleus, though the absolute values of the radii are too small due to a lack of repulsion in the effective NN interaction, the ratio of matter and charge radii agrees within the error bars with data, i.e., the halo structure is well reproduced.

For the ^{7}He system apart from the very well-reproduced ground state, two broad excited states, not observed until now, are predicted.

To deduce the spectrum of ^{9}He in a scattering calculation of neutrons off the ^{8}He bound state and the first excited state in analogy to the way we proceeded for ^{5}He and ^{7}He in this work, it is necessary to improve the description of the ground state and especially the first excited state in order to reproduce its experimental excitation energy. The presented work demonstrates that for the goal one has to modify the effective NN interaction so that it becomes also suitable for nuclei containing a large number of neutrons. Work in this direction is under way.

[1] M. V. Zhukov, B. V. Danilin, D. V. Fedorov, J. M. Bang, I. J. Thompson, and J. S. Vaagen, Phys. Rep. **231**, 151 (1993).

[2] V. I. Kukulin, V. I. Krasnopolsky, and P. N. Sazonov, Nucl. Phys. **A453**, 365 (1986).

[3] Y. Suzuki, Nucl. Phys. **A528**, 395 (1991).

[4] W. C. Parke and D. R. Lehman, Phys. Rev. C **29**, 2319 (1984).

[5] S. Aoyama, S. Mukai, K. Kato, and K. Ikeda, Prog. Theor. Phys. **93**, 99 (1995).

[6] E. Hiyama and M. Kamimura, Nucl. Phys. **A588**, 35c (1995).

[7] S. Funada, H. Kameyama, and Y. Sakuragi, Nucl. Phys. **A575**, 93 (1994).

[8] A. Csótó, Phys. Rev. C **48**, 165 (1993).

[9] B. S. Pudliner, V. R. Pandharipande, J. Carlson, and R. B. Wiringa, Phys. Rev. Lett. **74**, 4396 (1995).

[10] I. Tanihata, D. Hirata, T. Kobayashi, S. Shimoura, K. Sugimoto and H. Toki, Phys. Lett. B **289**, 261 (1992).

[11] K. Varga, R. G. Lovas, and Y. Suzuki, Z. Phys. A **349**, 347 (1994); K. Varga, Y. Suzuki, and Y. Ohbayasi, Phys. Rev. C **50**, 189 (1994); Y. Suzuki, K. Arai, Y. Ohbayasi, and K. Varga, Nucl. Phys. **A588**, 15c (1995).

[12] K. Varga, Y. Suzuki, and R. G. Lovas, Nucl. Phys. **A571**, 447 (1994).

[13] H. M. Hofmann, in *Resonating Group Calculations in Light Nuclear Systems* Lisboa, Portugal, 1986, Proceedings of Models and Methods in Few-Body Physics, edited by L. S. Ferreira, A. C. Fonseca, and L. Streit, Lecture Notes in Physics Vol. 273 (Springer, Berlin, 1987), p. 243.

[14] C. Winkler and H. M. Hofmann, Phys. Rev. C. **55**, 684 (1997), the preceding paper.

[15] H. H. Hackenbroich, *Proceedings of the International Symposium on Present status and novel developments in the nuclear many-body-problem*, Rome, 1972, edited by F. Calogero and C. Ciofi degli Atti (Editrice Compositori, Bologna, 1973) p. 706.

[16] T. Mertelmeier and H. M. Hofmann, Nucl. Phys. **A459**, 387 (1986).

[17] M. Unkelbach and H. M. Hofmann, Phys. Lett. B **261**, 211 (1991).

[18] S. Weber, M. Kachelriess, M. Unkelbach, and H. M. Hofmann, Phys. Rev. C **50**, 1492 (1994).

[19] B. Wachter, T. Mertelmeier, and H. M. Hofmann, Phys. Lett. B **200**, 246 (1988).

[20] J. Wurzer, Diploma thesis, Erlangen, 1994 (unpublished).

[21] K. Varga and Y. Suzuki, Phys. Rev. C **52**, 2885 (1995); K. Varga and Y. Suzuki, Phys. Rev. A **53**, 1907 (1996).

[22] SAID, access via telnet: vtinte.phys.vt.edu, login: physics, password: quantum, experimental data file: NN944 Nucl.Nucl. 8/94, solution: SM9 4 0-1.6 GeV.

[23] J. Wurzer and H. M. Hofmann, Z. Phys. A **354**, 135 (1996).

[24] R C. Barrett and D. F. Jackson, *Nuclear Sizes and Structure* (Clarendon, Oxford, 1977), p. 146.

[25] D. R. Tilley, H. R. Weller, and G. M. Hale, Nucl. Phys. **A541**, 1 (1992).

[26] S. R. Neumaier, Ph.D. thesis, Darmstadt 1995 (unpublished).

[27] S. R. Neumaier *et al.*, Nucl. Phys. **A583**, 799c (1995).

[28] S. R. Neumaier *et al.*, Proceedings of the International Conference on Exotic Nuclei and Atomic Masses, ENAM, Arles, France 1995, GSI Report No. GSI-95-33, 1995 (unpublished); G. D. Alkhazov *et al.*, Phys. Rev. Lett. (unpublished).

[29] O. G. Grebenjuk, A. V. Khanzadeev, G. A. Korolev, S. I. Manayenkov, J. Saudinos, G. N. Velichko, and A. A. Vorobyov, Nucl. Phys. **A500**, 637 (1989).

[30] F. Ajzenberg-Selove, Nucl. Phys. **A490**, 1 (1988).

[31] S. Ali, A. A. Z. Ahmed, and N. Ferdous, Rev. Mod. Phys. **57**, 923 (1985).

[32] I. Reichstein and Y. C. Tang, Nucl. Phys. **A158**, 529 (1970).

[33] T. Kobayashi, Nucl. Phys. **A538**, 343c (1992).

[34] P. G. Hansen and B. Jonson, Europhys. Lett. **4**, 409 (1987).

[35] Y. Ogawa, K. Yabana, and Y. Suzuki, Ref. [8] in [10].

[36] H. M. Hofmann, W. Zahn, and H. Stöwe, Nucl. Phys. **A357,** 139 (1981).

[37] H. Stöwe and W. Zahn, Nucl. Phys. **A289**, 317 (1977).

[38] W. von Oertzen *et al.*, Nucl. Phys. **A588**, 129c (1995).

[39] N. A. F. M. Poppelier, L. D. Wood, and P. W. M. Glaudemans, Phys. Lett. **157B**, 120 (1985).